A Study of Adducts Involving Dimethyl Sulfide Radical Cations and Methyl Halides: Experiment, Density Functional Theory, and Unimolecular Kinetic Modeling. 2c−3e Bonding vs Hydrogen Bonding

Linda S. Nichols and Andreas J. Illies*

Contribution from the Department of Chemistry, Auburn University, Alabama 36849-5312

Received April 19, 1999

Abstract: An experimental study of the ion/molecule association reactions in mixtures of methyl halide and dimethyl sulfide has been performed. MS/MS metastable and collision-induced dissociation experiments were performed on each $[C_3H_9SX]^{\bullet+}$ association product (X = I, Br, Cl, F) in order to determine structural conformations and to investigate reaction fragmentation pathways. For X = I, Br, and Cl, a two-center three-electron atomic connectivity for the association adduct giving the following structure $[CH_3X\therefore S(CH_3)_2]^+$ was observed. For X = F, the data suggests an F−H−S-bonded association adduct, $[CH_2F-H-S(CH_3)_2]^{\bullet+}$. Kinetic energy release distributions were measured for metastable products whenever possible. Furthermore, density functional theory and unimolecular kinetic modeling were carried out to further probe the potential energy surfaces of these radical cations.

Introduction

Two-center three-electron (2c−3e) bonding is a covalent type bonding interaction that was first suggested by Linus Pauling.[1] Two electrons from the highest occupied molecular orbital (HOMO) of a molecule interact with a single electron in a singly occupied molecular orbital (SOMO) of a radical to form a 2c−3e bond. The 2c−3e bond consists of a total of three electrons, two in a bonding orbital and one in an antibonding orbital. This gives a formal bond order of one-half, yielding a net bonding effect. The 2c−3e bond, therefore, has effectively one bonding electron. However, due to the greater destabilization of the antibonding orbital relative to the stabilization of the bonding orbital, a bond order of less than one-half is expected.[2]

In addition, the overall stability of the 2c−3e bond does not vary linearly with orbital overlap. Instead, as orbital overlap becomes more positive, the destabilization of the σ^* antibonding orbital increases relative to the stabilization of the σ bonding orbital until no net bonding remains.[3] Furthermore, it is more difficult to form a stable 2c−3e-bonded association adduct between species where ionization energies (IE) differ than between two species having the same ionization energies. Our group has studied the formation of these 2c−3e bonds within the methyl halide and mixed methyl halide systems[4−6] as well as the symmetric and unsymmetric 2c−3e bonding between alkyl sulfides.[7−10] These studies support the idea that, as the difference in ionization energy (ΔIE) increases, the 2c−3e bond strength decreases. Studies have also shown that the 2c−3e bond strength appears to decrease with increases in the electronegativity difference between the atoms forming the 2c−3e interaction.[11]

Previous theoretical studies on association ions suggest that, for interactions between second row elements, association adducts preferentially form through hydrogen bonding rather than a 2c−3e bond, while interactions involving third row elements form through either hydrogen bonding or 2c−3e bonds.[12] Our experimental studies on the association adducts formed between methyl halides appear to support this observation.[4,5] In this study, the following association reaction was examined for the formation of 2c−3e-bonded association products:

$$(CH_3)_2S^{\bullet+} + CH_3X \rightarrow [C_3H_9SX]^{\bullet+} \qquad (1)$$

X = I, Br, Cl, F. In reaction 1, the two reacting species have different IEs, and hence, the interacting MOs have different energies. The results of our attempts at forming unsymmetric 2c−3e-bonded adducts, $[(CH_3)_2S\therefore XCH_3]^+$, are given in this paper. The data have been carefully scrutinized in order to identify the type of interaction forming the association ion.

(1) Pauling, L. J. *J. Am. Chem. Soc.* **1931**, *53*, 3225.
(2) Young, D. C.; McKee, M. L. *Recent Trends in Computational Chemsitry*; Vol. 4 in press.
(3) Asmus, K.-D. *Acc. Chem. Res.* **1979**, *12*, 436.
(4) Nichols, L. S.; Illies, A. J. *Int. J. Mass Spectrom. Ion Processes* **1988**, *185/186/187*, 413.
(5) Nichols, L. S.; McKee, M. L.; Illies, A. J. *J. Am. Chem. Soc.* **1998**, *120*, 1538.
(6) Livant, P.; Illies, A. J. *J. Am. Chem. Soc.* **1991**, *113*, 1510.
(7) Deng, Y.; Illies, A. J.; James, M. A.; McKee, M. L.; Peschke, M. *J. Am. Chem. Soc.* **1995**, *117*, 420.
(8) Illies, A. J.; Nichols, L. S.; James, M. A. *J. Am. Soc. Mass Spectrom.* **1997**, *8*, 605.
(9) Illies, A. J.; Livant, P.; McKee, M. L. *J. Am. Chem. Soc.* **1988**, *110*, 7980.
(10) James, M. A.; Illies, A. J. *J. Phys. Chem.* **1996**, *100*, 15794.
(11) Chatgilialoglu, C., Asmus, K.-D., Eds. *Sulfur-Centered Reactive Intermediates in Chemistry and Biology*; Plenum Press: New York, 1990.
(12) Gill, P. M.; Radom, L. *J. Am. Chem. Soc.* **1988**, *110*, 4931.

10.1021/ja991246a CCC: $18.00
Published on Web 09/17/1999

Experimental Methods

All chemicals used in these experiments were commercially available. Samples were outgassed using several freeze−pump−thaw cycles and then dried on molecular sieves which had been baked out at temperatures slightly higher than 200 °C. The samples were transferred to, and stored in, glass bulbs which had been baked out by flaming with a torch under vacuum. Samples were introduced from these bulbs into the inlet line via Granville-Phillips Series 203 leak valves and were allowed to mix in the inlet line.

MS/MS experiments on the $[C_3H_9SX]^{\bullet+}$ association products were carried out with a modified VG-ZAB 1F mass spectrometer. The ion source, which allows for both electron ionization (EI) and chemical ionization (CI) studies, and the MS/MS collision cell modifications have been described in depth in previous publications.[8,10] Association ions were formed via ion/molecule reactions in the ion source using the CI slit at a temperature of approximately 400 K and an ionizing electron energy of 70 eV. Total source pressures were near 0.1 Torr. An excess of the sample with the highest IE was used in these experiments, and the ratio of the pressures was varied in order to maximize the signal.

Metastable scans were carried out in the second field-free region at a base pressure of 2×10^{-8} Torr using multiple scanning methods. Kinetic energy release distributions (KERD) were obtained from the metastable peaks shape by published methods.[13] Collision-induced dissociation (CID) spectra were also recorded in the second field-free region with a peak attenuation of 40% using helium as a collision gas.

Computational Methods

DFT Calculations. All calculations on the association radical cations and tight transition states were performed using the Gaussian 94 program system.[14] The geometry of each species was first optimized at the AM1 level and then used as the input for the density functional theory (DFT) calculations at the B3LYP/6-31+G(d,p) level of theory. The nature of the stationary points was checked by calculating vibrational frequencies. The calculated electron densities were carefully inspected to ensure the nature of the association radical cations, specifically to distingush between 2c−3e bonds and electrostatic interactions by checking for delocalization of the electrons between the two interacting moieties. Although an ion/dipole interaction might be expected to yield experimental results similar to some of those obtained in this study, the DFT calculations and kinetic modeling support the existence of the 2c−3e bond.

In accordance with our previous methyl halide studies,[4,5] a quasirelativistic effective core potential developed by Bergner et al.[15] was used for the core electrons of bromine and iodine while the valence electrons were described with a 311/311/1 basis set contraction. The basis set contraction was obtained by adding an additional s primitive and d primitive to the set proposed by Bergner. The s and d primitives were taken from Dolg's larger valence set;[16] the method by which they were chosen has been described in a previous study.[4]

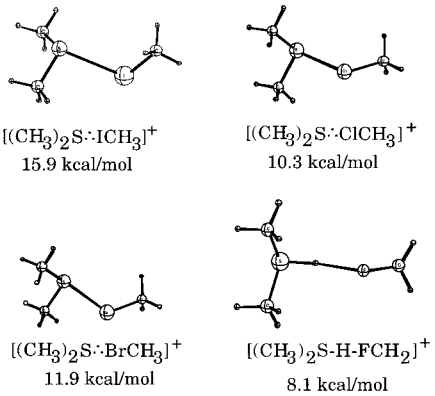

Figure 1. DFT minimum energy structures for sulfur−halide association radical cations.

Unimolecular Kinetic Modeling. Phase space programs developed and supplied by Bowers and co-workers were used in the unimolecular kinetic modeling studies.[17] The use of phase space theory in modeling reactions involving a tight transition state for rearrangement combined with a loose orbiting transition state for the final step in the reaction has been shown to be valid only if, after passing through the tight transition state, the trajectories remain statistical up to the orbiting transition state.[18] The phase space programs model the experimentally measured KERDs and provide insight on the potential energy surfaces (PES) and fragmentation pathways for each adduct. The parameters for the orbiting transition states such as rotational constants, vibrational frequencies, and energies used in the phase space calculations were taken from previous computational results;[4,5] however, parameters for the association adducts were taken from the aforementioned DFT calculations while polarizabilities were taken from the literature.[19] Collision complex energies and angular momentum distributions were determined by thermal ion/molecule collision theory.[20] The energies of the tight transition were estimated by adjusting the energies in order to fit the experimentally measured KERDs; this has been shown to be valid in previous studies by Bowers et al.[18] For all modeling presented here, transition states having energies −0.10 eV relative to the reactant species resulted in the best fits. All molecular parameters used for the phase space modeling have been provided as Supporting Information.

Results and Discussion

Although a comprehensive study of the potential energy surfaces for the reactions studied here was not undertaken, all association structures proposed in this study were examined by DFT. The proposed association products were found to be strongly bonded relative to reactants, and both their minimum energy structures and corresponding bond strengths are given in Figure 1. The 2c−3e-bonded species have C_1 symmetry, and the 2c−3e bond lengths were found to be 3.21 Å for S∴I, 3.03 Å for S∴Br, and 2.97 Å for S∴Cl, consistent with a 2c−3e sulfur−halide bond being present.[2]

$[(CH_3)_2S\therefore ICH_3]^+$ and $[(CH_3)_2S\therefore {}^{81}BrCH_3]^+$. The metastable spectrum of $[(CH_3)_2S\therefore ICH_3]^+$ (Figure 2) shows two

(13) Jarrold, M. F.; Illies, A. J.; Kirchner, N. J.; Wagner-Redecker, W.; Bowers, M. T.; Maudich, M. L.; Beauchamp, J. L. *J. Phys. Chem.* **1983**, *87*, 2213.

(14) Frisch, M. J.; Trucks, G. W.; Schlegel, H. B.; Gill, P. M. W.; Johnson, B. G.; Robb, M. A.; Checseman, J. R.; Kieth, T.; Petersson, G. A.; Montgomery, J. A.; Ragharachari, K.; Allaham, M. A.; Zakrzewski, V. G.; Ortiz, J. V.; Foresmar, J. B.; Cioslowski, J.; Stefanov, B. B.; Nanayakkara, A.; Challacombe, M.; Peng, C. Y.; Ayala, P. V.; Chen, W.; Martin, J.; Stewart, J. P.; Head-Gordon, M.; Gonzalez, C.; Pople, J. A. Gaussian 94 (rev. B.1), Gaussian, Inc. Pittsburgh, PA, 1995.

(15) Bergner, A.; Dolg, M.; Kuchle, W.; Stoll, H.; Preuβ, H. *Mol. Phys.* **1993**, *80*, 1431.

(16) Dolg, M. database at http://www.theochem.uni-stuttgart.de/.

(17) Carpenter, C. J.; Van Koppen, P. A. M.; Bowers, M. T.; *J. Am. Chem. Soc.* **1995**, *117*, 10976.

(18) Hanratty, M. A.; Beauchamp, J. L.; Illies, A. J.; Van Koppen, P.; Bowers, M. T. *J. Am. Chem. Soc.* **1988**, *110*, 1.

(19) Lide, D. R., Ed. *CRC Handbok of Chemistry and Physics*; CRC Press: Boca Raton, Florida, 1994.

(20) Bass, L. M.; Cates, R. D.; Jarrold, M. F.; Kirchner, N. J.; Bowers, M. T. *J. Am. Chem. Soc.* **1983**, *105*, 7024.

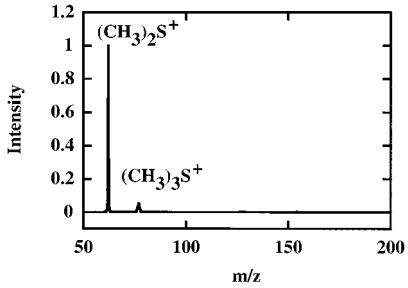

Figure 2. MS/MS metastable spectrum of $[(CH_3)_2S\therefore ICH_3]^+$.

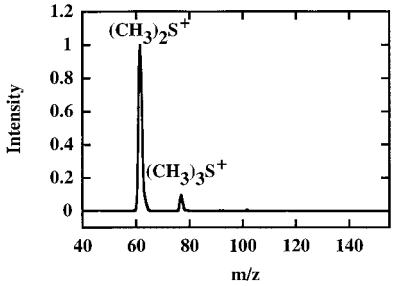

Figure 3. MS/MS metastable spectrum of $[(CH_3)_2S\therefore {}^{81}BrCH_3]^+$.

daughter peaks, $(CH_3)_2S^{\bullet+}$, *m*/*z* 62, and $[(CH_3)_2S-CH_3]^+$, *m*/*z* 77, which result from reactions 2 and 3, respectively.

$$[(CH_3)_2S\therefore ICH_3]^+ \rightarrow (CH_3)_2S^{\bullet+} + CH_3I \qquad (2)$$

$$[(CH_3)_2S\therefore ICH_3]^+ \rightarrow [(CH_3)_2S-CH_3]^+ + I^{\bullet} \qquad (3)$$

Of the two peaks, $(CH_3)_2S^{\bullet+}$, *m*/*z* 62, resulting from direct cleavage of the 2c−3e S∴I bond, is the most intense. The peak at *m*/*z* 77, $[(CH_3)_2S-CH_3]^+$, could only result from a structural rearrangement of the proposed 2c−3e-bonded $[(CH_3)_2S\therefore ICH_3]^+$ adduct with subsequent elimination of the iodine via reaction 3. We propose a rearrangement similar to that previously noted by our group in the symmetric methyl halide studies.[5] During the rearrangement, the S−I bond lengthens while the methyl group from the methyl iodide migrates and inserts into the S−I bond, forming a transition state with the following connectivity: $[(CH_3)_2S-CH_3-I]^{\bullet+}$. The I−C bond then continues to elongate until the products (reaction 3) are formed.

The metastable spectrum for $[(CH_3)_2S\therefore {}^{81}BrCH_3]^+$ is shown in Figure 3. As was the case with $[(CH_3)_2S\therefore ICH_3]^+$, two peaks, from the reactions given below, were observed.

$$[(CH_3)_2S\therefore BrCH_3]^+ \rightarrow (CH_3)_2S^{\bullet+} + CH_3Br \qquad (4)$$

$$[(CH_3)_2S\therefore BrCH_3]^+ \rightarrow [(CH_3)_2S-CH_3]^+ + Br^{\bullet} \qquad (5)$$

The KERDs obtained for the direct metastable fragmentation pathways given in reactions 2 and 4 are shown in Figures 4 and 6. The narrow distribution shapes in Figures 4 and 6 indicate that reactions 2 and 4 proceed via a direct fragmentation. The average kinetic energy release, KER, for $(CH_3)_2S^{\bullet+}$ from reaction 2 is 6.10 meV, while the average KER for $(CH_3)_2S^{\bullet+}$ from reaction 4 is 6.14 meV. The phase space modeling (solid continuous line shown in Figures 4 and 6) used orbiting transition states and surfaces with no reverse activation barriers. The results obtained are consistent with a direct fragmentation process involving a simple bond cleavage.

Figures 5 and 7 also show the KERDs for $[(CH_3)_2S-CH_3]^+$ resulting from reactions 3 and 5. These distributions are much broader than the KERDs for the direct cleavage reactions 2 and 4; the average KERs are 144.7 meV for reaction 3 and 186

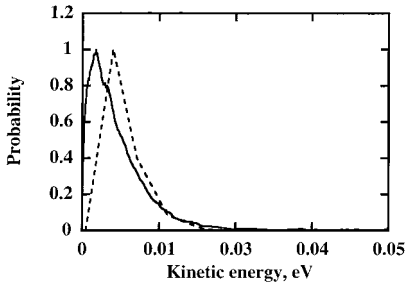

Figure 4. Metastable kinetic energy release distributions for $[(CH_3)_2S\therefore ICH_3]^+ \rightarrow (CH_3)_2S^{\bullet+} + CH_3I$ (reaction 2). Phase space results are shown by the dotted line.

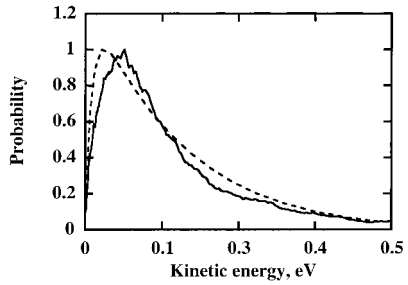

Figure 5. Metastable kinetic energy release distributions for $[(CH_3)_2S\therefore ICH_3]^+ \rightarrow (CH_3)_3S^+ + I^{\bullet}$ (reaction 3). Phase space results are shown by the dotted line.

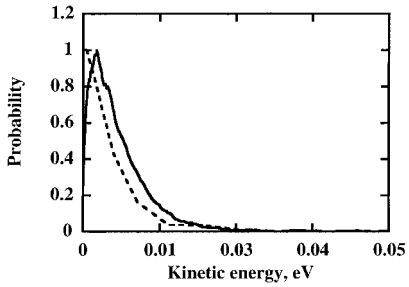

Figure 6. Metastable kinetic energy release distribution for $[(CH_3)_2S\therefore {}^{81}BrCH_3]^+ \rightarrow (CH_3)_2S^{\bullet+} + CH_3Br$ (reaction 4). Phase space results are shown by the dotted line.

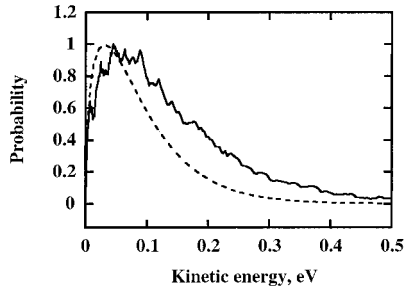

Figure 7. Metastable kinetic energy release distributions for $[(CH_3)_2S\therefore BrCH_3]^+ \rightarrow (CH_3)_3S^+ + Br^{\bullet}$ (reaction 5). Unimolecular kinetic modeling is indicated by the dotted line.

meV for reaction 5. Both large reverse activation barriers and rearrangement processes could contribute to the larger KERDs.[17] Unimolecular kinetic modeling studies used tight transition states for the rearrangements and loose orbiting transition states for the final step in the reactions.[18] The modeled results are in good agreement with the experimentally measured KERDs. These results support the rearrangement and subsequent elimination of a halide as suggested for reactions 3 and 5.

The CID results for $[(CH_3)_2S\therefore ICH_3]^+$ are given in Figure 8. The most intense peaks in this spectrum are $(CH_3)_2S^{\bullet+}$, *m*/*z* 62, $CH_3I^{\bullet+}$, *m*/*z* 142, and $[(CH_3)_2SI]^+$, *m*/*z* 189. All three peaks

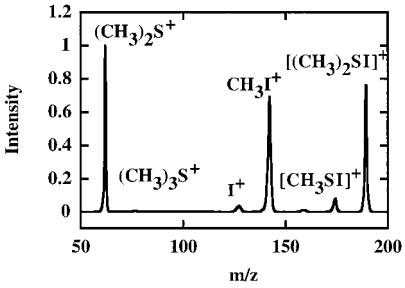

Figure 8. Collision-induced dissociation spectrum of $[(CH_3)_2S\therefore ICH_3]^+$.

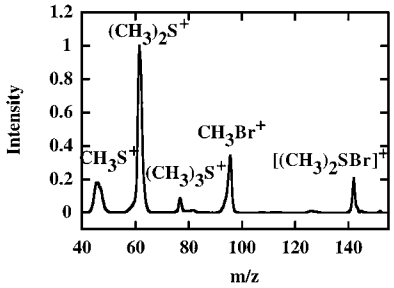

Figure 9. Collision-induced dissociation spectrum of $[(CH_3)_2S\therefore {}^{81}BrCH_3]^+$.

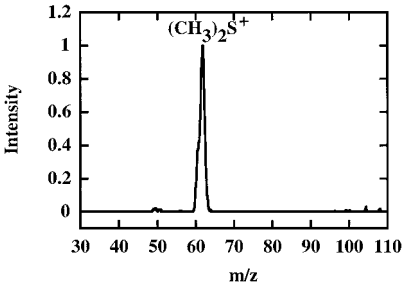

Figure 10. Metastable spectrum of $[(CH_3)_2S\therefore {}^{35}ClCH_3]^+$.

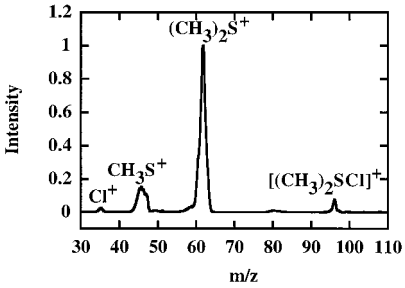

Figure 11. Collision-induced dissociation spectrum of $[(CH_3)_2S\therefore {}^{35}ClCH_3]^+$.

result from direct bond cleavage processes. Of these three peaks, $(CH_3)_2S^{\bullet+}$ and $CH_3I^{\bullet+}$ arise from the fragmentation of the 2c−3e bond with $(CH_3)_2S^{\bullet+}$ having a higher intensity due to its lower IE. $[(CH_3)_2S-CH_3]^+$, one of the peaks present in the metastable spectrum, is very weak relative to $(CH_3)_2S^{\bullet+}$ in the CID spectrum. This is because, in CID, direct cleavage reactions occur on a faster time scale than do rearrangement reactions.[21−23] The remaining peaks, I^+, *m*/*z* 127; SI^+, *m*/*z* 159; CH_3S^+, *m*/*z* 47; and $CH_2S^{\bullet+}$, *m*/*z* 46, are much less intense as expected due to the larger number of bonds being broken. It is interesting to note that a very weak peak for SI^+ at *m*/*z* 159 is observed; this provides relatively strong evidence of the S−I atomic connectivity in the $[(CH_3)_2S\therefore ICH_3]^+$ radical cation.

The CID spectrum for $[(CH_3)_2S\therefore BrCH_3]^+$ is presented in Figure 9. As with the $[(CH_3)_2S\therefore ICH_3]^+$ case, the three most intense peaks in the spectrum, $(CH_3)_2S^{\bullet+}$, $CH_3Br^{\bullet+}$, and $[(CH_3)_2S-Br]^+$, derive from direct bond cleavage. Of these, $[(CH_3)_2S]^{\bullet+}$ is the most intense and results from the direct cleavage of the 2c−3e bond. Also arising from this bond cleavage is $CH_3Br^{\bullet+}$, *m*/*z* 96, which is much less intense in the spectrum due to the higher IE of neutral CH_3Br compared to $(CH_3)_2S$. Other peaks present include $[(CH_3)_2S-CH_3]^+$, *m*/*z* 77; CH_3S^+, *m*/*z* 47; $CH_2S^{\bullet+}$, *m*/*z* 46; and Br^+, *m*/*z* 81. Unlike the CID spectrum for $[(CH_3)_2S\therefore ICH_3]^+$, SBr^+, *m*/*z* 113, is not seen; however, the $[(CH_3)_2S\therefore BrCH_3]^+$spectrum is consistent with a 2c−3e S∴Br atomic connectivity. As discussed in the Introduction, the larger the ΔIE, the weaker the 2c−3e bond. Therefore, the S∴Br bond would be expected to be weaker and more easily broken than the S∴I bond (ΔIE = 1.85 eV vs ΔIE = 0.85 eV).[24] In fact, the DFT calculated bond energies support this with bond energies of 15.9 and 11.9 kcal/mol (see Figure 1). This helps explain the absence of SBr^+ in the CID spectrum of $[(CH_3)_2S\therefore BrCH_3]^+$ as opposed to the presence of SI^+ in the CID spectrum of $[(CH_3)_2S\therefore ICH_3]^+$.

$[(CH_3)_2S\therefore {}^{35}ClCH_3]^+$. The metastable spectrum of $[(CH_3)_2S\therefore ClCH_3]^+$ is shown in Figure 10. Unlike the previous spectra, there is only one peak present, $(CH_3)_2S^{\bullet+}$, *m*/*z* 62, for the metastable fragmentation pathway of the $[(CH_3)_2S\therefore ClCH_3]^+$ association adduct. Because of interference from a neighboring peak which broadened the $(CH_3)_2S^{\bullet+}$ peak, we were unable to measure the KERD for this metastable process.[25]

The most intense peak present in the CID spectrum for the $[(CH_3)_2S\therefore ClCH_3]^+$, *m*/*z* 112, system (Figure 11) is $(CH_3)_2S^{\bullet+}$, *m*/*z* 62. A peak observed in this spectrum, $[(CH_3)_2SCl]^+$, *m*/*z* 97, results from a direct cleavage reaction resulting in elimination of a methyl group. Cl^+, *m*/*z* 35; CH_3S^+, *m*/*z* 47; and $CH_2S^{\bullet+}$, *m*/*z* 46, originate via multiple bond cleavages. While we do observe Cl^+, there is no $CH_3Cl^{\bullet+}$, *m*/*z* 50, present. This probably arises from the dynamics of the 2c−3e bond cleavage; the CH_3Cl has a much higher IE than $(CH_3)_2S$ (11.22 eV as compared to 8.69 eV),[24] and the charge appears to reside chiefly on the $(CH_3)_2S$ moiety upon fragmentation. The CID spectrum supports the 2c−3e, $[(CH_3)_2S\therefore ClCH_3]^+$, atomic connectivity.

It is interesting to note that as ΔIE increases and the 2c−3e bond energy decreases, the intensity of the CID $CH_3X^{\bullet+}$ peak decreases relative to the intensity of $(CH_3)_2S^{\bullet+}$ (see Figures 8, 9, and 11). The 2c−3e bond strength is expected to decrease with increasing ΔIE; however, 2c−3e bond energies have also been observed to decrease with increasing differences in electronegativity (ΔEN), consistent with the results reported here (Table 1).[4] The S∴X bond strengths in these systems decrease in the order SI > SBr > SCl (see DFT results presented in

(21) Jennings, K. R. *Int. J. Mass Spectrom. Ion Phys.* **1968**, *1*, 227.

(22) McLafferty, F. W.; Bente, P. F., III; Kornfeld, R.; Tsai, S. C.; Howe, I. *J. Am. Chem. Soc.* **1973**, *95*, 2120.

(23) Cooks, R. G.; Beynon, J. H.; Caprioli, R. M.; Lester, G. R. *Metastable Ions*; Elsevier Scientific Pub. Co.: Amsterdam, The Netherlands, 1973.

(24) Lias, S. G.; Bartmess, J. E.; Liebman, J. F.; Holmes, J. L.; Levin, R. D.; Mallard, W. G. *Journal of Physical and Chemical Reference Data*; American Chemical Society and the American Institute of Physics for the National Bureau of Standards: New York, 1988.

(25) (a) Heerma, W.; Sarneel, M. M.; Terlouw, J. K. *Org. Mass Spectrom.* **1981**, *16*, 325. Interference peaks originating from neighboring masses have been documented; they can be observed in MIKES scans if there is an intense parallel beam of a neighboring mass after momentum analysis in the second field free region. If fragment ions from the neighboring beam have sufficient kinetic energy, they can appear in the MIKES spectrum of the mass of interest as interference peaks. To test for these interference peaks, one can tune the magnet for maximum interference peak intensity. Interference peaks increase in intensity relative to genuine fragment ions as the magnetic field approaches that for the proper passage of the interference parent ion, resulting in a "cross over" to the neighboring parent beam.

Table 1. Computational Bond Energies (eV) of Unsymmetric 2c−3e Bonds Formed between Alkyl Halides and Dialkyl Sulfides

species	energies (eV)[a]	ΔIE (eV)[b]	ΔEN (eV)[c]	KER (meV)
$[Me_2S\therefore SMe_2]^{\bullet+}$	1.19	0	0.00	21
$[(CH_3)_2S\therefore ICH_3]^{\bullet+}$	0.69	0.84	0.08	6.10
$[(CH_3)_2S\therefore BrCH_3]^{\bullet+}$	0.52	1.85	0.38	6.14
$[(CH_3)_2S\therefore ClCH_3]^{\bullet+}$	0.45	2.53	0.58	
$[(CH_3)_2S\therefore FCH_3]^{\bullet+}$		3.78	1.40	

[a] Zero point energies have been included. [b] IEs taken from ref 24 in text. [c] Electronegativities are from Shriver, D. F.; Atkins, P.; Langford, C. H. *Inorganic Chemistry;* W. H. Freeman and Company: New York, 1994; p 44.

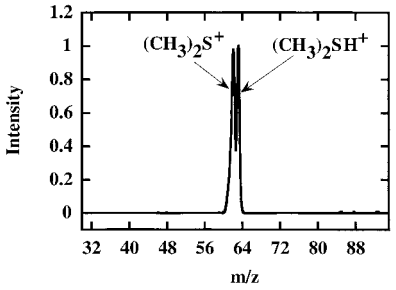

Figure 12. Metastable spectrum of $[C_3H_9SF]^{\bullet+}$.

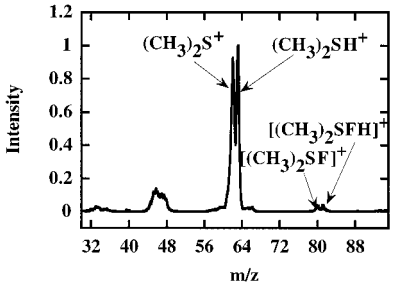

Figure 13. Collision-induced dissociation spectrum of $[C_3H_9SF]^{\bullet+}$.

Figure 1). It appears that formation of $(CH_3)_2S^{\bullet+}$ is the dominant process upon cleavage of the 2c−3e bond and the intensity of this peak is so great that other peaks originating from direct cleavage processes are less intense. Due to the low IE of CH_3Cl as compared to $(CH_3)_2S$, $CH_3Cl^{\bullet+}$ is not observed.

$[C_3H_9SF]^{\bullet+}$. The metastable spectrum for $[C_3H_9SF]^{\bullet+}$ is given in Figure 12. There are 2 peaks present in this spectrum, $(CH_3)_2S^{\bullet+}$, *m/z* 62, and $(CH_3)_2SH^+$, *m/z* 63. While both peaks could result from a 2c−3e-bonded species, it has been previously noted that 2c−3e bond strength decreases with large differences in electronegativity and a 2c−3e-bonded adduct might not be expected. The similar intensity of the $(CH_3)_2SH^+$ and $(CH_3)_2S^{\bullet+}$ peaks suggests that they both result from a direct cleavage reaction; hence, they may originate from a hydrogen-bonded adduct. This is not suprising since association ions have been noted to predominately form through hydrogen-bonding interactions for second row elements.[12] The two metastable peaks in the spectrum are not completely resolved and prevented measurement of the KERDs.

Similar to the metastable spectrum, the CID spectrum (Figure 13) shows $(CH_3)_2S^{\bullet+}$, *m/z* 62, and $(CH_3)_2SH^+$, *m/z* 63, as intense peaks. Weaker peaks are also present in this spectrum at $[(CH_3)_2SFH]^+$, *m/z* 82, CH_2F^+, *m/z* 33, $[(CH_3)_2SF]^+$, *m/z* 81 (this designation is not meant to indicate structure), CH_3S^+, *m/z* 47, and CH_2S^+, *m/z* 46. The peaks at $[(CH_3)_2SFH]^+$, *m/z* 82, and CH_2F^+, *m/z* 33, in addition to the $(CH_3)_2SH^+$ peak, seem to indicate the presence of a F−H−S-bonded $[H_2CF-H-S(CH_3)_2]^{\bullet+}$ structure. $[(CH_3)_2SFH]^{\bullet+}$, *m/z* 82, could be formed from this adduct by cleavage of the C−F bond, while cleavage of the F−H bond would be required to form either CH_2F^+ or $(CH_3)_2SH^+$. This particular type of ylidium structure has been observed in previous methyl halide studies involving CH_3F and CH_3Cl.[4,5,26] The peak at *m/z* 81 most likely results from the loss of a methyl group from $[H_2CF-H-S(CH_3)_2]^{\bullet+}$ to form $[CH_3S-H-FCH_2]^+$. Both the metastable and CID spectra of $[C_3H_9SF]^{\bullet+}$ indicate a hydrogen-bonded adduct rather than a 2c−3e-bonded adduct. DFT calculations resulted in a stable structure for $[(CH_3)_2S-H-FCH_2]^{\bullet+}$ (Figure 1).

Previous experiments with CH_3Cl and CH_3F[4,5,26] show that these species often undergo ion/molecule reactions to form hydrogen-bonded association radical cations rather than 2c−3-bonded dimers. The hydrogen bond is known to be one of the strongest *inter*molecular bonds formed in nature. A hydrogen bond formed between two neutral molecules usually has a bond strength between 15 and 40 kJ/mol.[27] However, hydrogen bonds formed in radical cations have been shown to have bond strengths up to 116 kJ/mol. This increase in stability is attributed to ion−dipole interactions.[28] Strong hydrogen bonds are known to form between the H atom, which is already bonded to a highly electronegative atom and the highly electronegative F, O, or N atoms of a neighboring molecule. In some cases, hydrogen bonds occur between the H atom and a Cl or S atom of a neighboring molecule. These hydrogen-bonding interactions are important in biological systems; however, the bonds are weaker than the strong hydrogen bonds that form with F, N, or O. The formation of $[H_2CF-H-S(CH_3)_2]^{\bullet+}$ in this study and similar structures formed in previous studies with CH_3F seems to suggest that, sometimes, hydrogen-bonding interactions are preferred over 2c−3e-bonding interactions for ion/molecule association reactions involving CH_3F.

We have noted the propensity for formation of $CH_2S^{\bullet+}$, *m/z* 46, in the CID spectra for all species studies; however, we do not, at present, understand its origin. It is possible that $CH_2S^{\bullet+}$ results from multiple CID.

Conclusions

There are two metastable fragmentation pathways for the $[(CH_3)_2S\therefore XCH_3]^+$ systems when X = I, Br. The small average KERs for reactions 2 and 4 are consistent with direct cleavage by a statistical unimolecular process with a small or no reverse activation barrier. The larger average KERs obtained for reactions 3 and 5 indicate that a structural rearrangement process occurs prior to the elimination of the halide. The ability to model the KERDs for each of these systems supports the proposed fragmentation pathways. The metastable and CID spectra support the presence of a 2c−3e-bonded $[(CH_3)_2S\therefore XCH_3]^+$ structure.

Metastable experiments indicate that there is only one fragmentation pathway for the $[(CH_3)_2S\therefore ClCH_3]^+$ adduct; however, CID experiments on this ion support the S∴Cl atomic connectivity. In contrast, the metastable and CID experiments for the $[C_3H_9SF]^{\bullet+}$ radical cation give evidence of an isomer with a different atomic connectivity. The spectra are consistent with the hydrogen-bonded structure, $[(CH_3)_2S\text{-}H\text{-}FCH_2]^{\bullet+}$. It is believed that such hydrogen-bonded species may be the preferred bonding interaction for ion/molecule association reactions involving CH_3F and $(CH_3)_2S$.

(26) de Visser, S. P.; de Koning, L. J.; Nibbering, N. M. M. *J. Am. Chem. Soc*. **1998**, *120*, 1517.

(27) Petrucci, R. H. *General Chemistry: Principles and Modern Applications*; Macmillan Publishing Co.: New York, New York, 1989.

(28) de Visser, S. P. Dissertation: Dimer Radical Cations in the Gas-Phase, Institute of Mass Spectrometry, University of Amsterdam, 1997.

Acknowledgment. A.J.I. would like to express his appreciation to BASF for the donation of the ZAB 1F (serial no. 120). L.S.N. is grateful to the USDE for a Graduate Assistance in Area of National Needs (GAANN) Fellowship and to the Auburn University Chemistry Department and Mrs. Samuel Nichols for a Nichols Fellowship.

Supporting Information Available: Tables containing the input parameters for the phase space calculations. This material is available free of charge via the Internet at http://pubs.acs.org.

JA991246A